ACS APPLIED MATERIALS & INTERFACES

Research Article

www.acsami.org

# Ultraviolet $ZnSe_{1-x}S_x$ Gradient-Alloyed Nanocrystals via a Noninjection Approach

Kui Yu,*[,†] Amy Hrdina,[†] Jianying Ouyang,[†] David Kingston,[‡] Xiaohua Wu,[§] Donald M. Leek,[†] Xiangyang Liu,[†] and Chunsheng Li[∥]

[†]Steacie Institute for Molecular Sciences, National Research Council of Canada, Ottawa, Ontario K1A 0R6, Canada

[‡]Institute for Chemical Process and Environmental Technology, National Research Council of Canada, Ottawa, Ontario K1A 0R6, Canada

[§]Institute for Microstructural Sciences, National Research Council of Canada, Ottawa, Ontario K1A 0R6, Canada

[∥]Healthy Environment and Consumer Safety Branch, Health Canada, Ottawa, Ontario, K1A 1C1, Canada

Supporting Information

**ABSTRACT:** Highly emissive ultraviolet ZnSeS nanocrystals (NCs), with a core–shell-like structure, were designed and synthesized via a one-step noninjection approach in 1-octadecene (ODE). These ultraviolet ZnSeS NCs exhibit bright bandgap emission with high color purity and little trap emission. With full width at half-maximum (fwhm) of ~21 nm only, photoluminescent (PL) quantum yield (QY) of ~60% was estimated for one ensemble dispersed in toluene exhibiting bandgap absorption peaking at ~380 nm and bandgap emission at ~389 nm. These alloyed ZnSeS NCs present a cubic crystal structure consisting of a Se-rich core and a S-rich shell. Such a gradiently alloyed structure was suggested by our investigation on the temporal evolution of optical properties of the growing ZnSeS NCs monitored from 80 to 300 °C, together with structural and compositional characterization performed with XRD, XPS, EDX, and TEM. This newly developed one-step noninjection approach was achieved with zinc oleate ($Zn(OA)_2$), diphenylphosphine selenide (SeDPP), and diphenylphosphine sulfide (SDPP) as Zn, Se, and S precursors, respectively. ZnSe monomers mainly participated in nucleation at ~120 °C, while both ZnSe and ZnS monomers contributed to NC formation in later growth stages (~160 °C and higher). $^{31}P$ NMR study demonstrates that SeDPP is more reactive than SDPP toward $Zn(OA)_2$, and also supports such a model proposed on the combination of ZnSe and ZnS monomers leading to nucleation/growth of ZnSeS alloyed NCs. The present study offers conceptual methodology to various highly photoluminescent alloyed NCs with high quality, high particle yield, and high synthetic reproducibility.

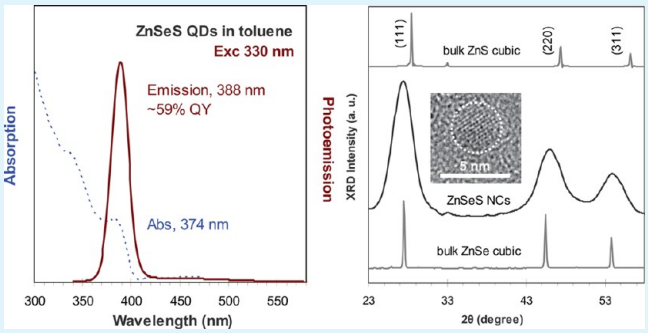


**KEYWORDS:** *alloyed ZnSeS nanocrystals, colloidal quantum dots, photoluminescent, diphenylphosphine, noninjection approach*

## 1. INTRODUCTION

The bandgap engineering of colloidal semiconductor nanocrystals (NCs) exhibiting blue or ultraviolet bandgap absorption and emission via a noninjection approach has received significant attention in our laboratories,[1] due to their technological potential in optoelectronics including light-emitting diodes (LEDs) and laser diodes (LD).[2−11] Short wavelength emitters are in demand for high-performance light-emitting devices, high-density compact-optical-storage-disk systems, and laser printers. Storage density amplifies proportionally to the square of light source wavelength, and the density of printed dots increases with the decrease of the wavelength of a laser used. Meanwhile, the endeavor of our synthetic development via a noninjection approach[1,12−17] is concomitant with our fundamental interest in monomers and their combination leading to nucleation and growth of colloidal NCs.[1,12−14,18−25]

The use of secondary phosphine, diphenylphosphine (DPP), has been acknowledged to promote particle yields since 2006.[19] Recently, we reported the use of secondary phosphine, diphenylphosphine (DPP), to promote the reactivity of precursors for an enhancement of particle yields of small-sized PbSe NCs and for the formation of alloyed PbSeS NCs.[12−14] For the latter, we used a low-cost and air-stable thioacetamide (TAA) as a S source instead of expensive and air-sensitive bis(trimethylsilyl) sulphide.[14,26] Furthermore, we used a low-temperature noninjection approach with long growth periods such as 45 min at 60 °C instead of 90 s at 150 °C.[14,26] The resulting PbSeS NCs were of high quality, as demonstrated by Schottky-type solar cells fabricated with the PbSeS NCs as

Received: June 1, 2012
Accepted: July 6, 2012
Published: July 19, 2012

their active materials, exhibiting the highest power conversation efficiency of 3.44% as compared to the same type of solar cells with PbSeS NCs as their active layers.[14,26] At the same time, secondary phosphine selenide, diphenylphosphine selenide (SeDPP), has been acknowledged to be more reactive than tertiary phosphine selenide such as n-trioctylphosphine selenide (SeTOP), with much more nanocrystals generated and was used as a Se precursor to synthesize highly emissive Se-based NCs.[1,22,23,25]

Bandgap engineering could be achieved via the control of the size and composition of semiconductor NCs. The synthesis of alloyed NCs, the bandgap of which could be tuned at a constant size, is in its infancy.[14−17,27−36] At the same time, alloyed NCs were documented to exhibit better stability with bright photoluminescence (PL) than binary and core−shell systems, such as alloyed ZnCdSe versus binary CdSe and core−shell CdSe/ZnS NCs.[27,29]

Until now, alloyed ZnSeS NCs exhibiting bandgap emission have been reported scarcely.[37−39] It is noteworthy that Zn is a nontoxic element. Cubic zincblende ZnSe and ZnS are II−VI semiconductor materials, with small exciton Bohr radii of 4.5 and 2.2 nm, wide band gap of 2.70 eV (~460 nm) and 3.70 eV (~335 nm), and lattice constants of 0.5668 and 0.5406 nm at room temperature, respectively.[40−43] Such a small lattice mismatch promises a practical way to position S into the ZnSe lattice to form ZnSeS alloyed NCs with bright bandgap emission in the ultraviolet region. However, it has been an enduring challenge to prepare high-quality ZnSeS alloyed NCs with bright bandgap photoemission.

Herein, we report a noninjection-based one-pot approach in 1-octadecene (ODE) to ultraviolet luminescent ZnSeS NCs with a cubic structure and gradient distribution of elements consisting of a Se-rich core and a S-rich shell. On the basis of our noninjection approaches to ZnSe,[1] PbSeS,[14] ZnCdS,[15] and CdSeS,[17] this newly developed synthesis used zinc oxide, elemental selenium (Se), and elemental sulfur (S) as Zn, Se, and S sources, respectively. DPP was employed to prepare highly reactive Se and S precursors, SeDPP and diphenylphosphine sulfide (SDPP), respectively. Zinc oleate ($Zn(OA)_2$) was used as a Zn precursor. The addition of a mixture of the Se and S precursors to a Zn precursor solution in ODE was typically carried out at 80 °C with the growth in the temperature range of 80−300 °C. The temporal evolution of absorption and photoemission of growing NCs was monitored, indicating that the nucleation/growth kinetics of the resulting ternary $ZnSe_{1-x}S_x$ NCs, together with their composition and distribution of Se and S, were sensitive to experimental parameters such as SeDPP-to-SDPP feed molar ratios. Structural and compositional characterization by transmission electron microscopy (TEM), X-ray diffraction (XRD), X-ray photoelectron spectroscopy (XPS), and energy-dispersive X-ray spectroscopy (EDX) was performed. In addition, high-resolution $^{31}P$ NMR with $^{1}H$ decoupling was carried out to investigate the reactivity of SeDPP and SDPP as well as to bring insight into the formation mechanism of ZnSeS alloys via the combination of ZnSe and ZnS monomers, as shown in Scheme 1 and Supporting Information Figure S1.

## 2. RESULTS AND DISCUSSION

In general, our noninjection one-pot approach features high-quality ZnSeS NCs exhibiting bright ultraviolet bandgap emission, with excellent synthetic reproducibility and readiness to scale up. With a precursor feed molar ratio of $4Zn(OA)_2$−0.7SeDPP−0.3SDPP and feed [Se + S] of 60 mmol $kg^{-1}$, the resulting ZnSeS alloyed NCs dispersed in toluene after their growth at 300 °C exhibited sharp excitonic absorption (peaking at ~380 nm) and narrow photoluminescent (PL) emission (peaking at ~389 nm with 350 nm excitation) with full width at half-maximum (fwhm) of ~21 nm. As compared to 55% quantum yield (QY) of quinine sulfate in 0.05 M $H_2SO_4$ presented in Figure 1, this ensemble exhibited photoluminescent (PL) QY of ~60%. See Experimental Section for experimental details.

**Scheme 1. Schematic Drawing of the Formation of the Alloyed ZnSeS NCs via the Combination of the Two Monomers of ZnSe and ZnS[a]**

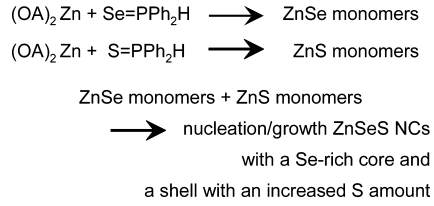


[a]The formation of $Ph_2P$-$PPh_2$ and DPP during the nanocrystal formation is noteworthy. The combination of monomers leading to nucleation and growth was proposed before for binary NC systems.[1,12,13,19−21,25,61]

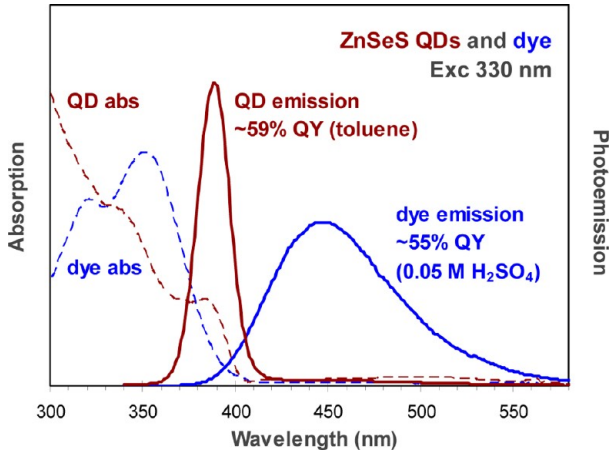


**Figure 1.** Emission efficiency of ZnSeS QDs in toluene (sample 12 of Figure 2 Batch 0.7SeDPP-0.3SDPP) is compared with that of a dye quinine sulfate. The emission spectra (solid lines with excitation wavelength of 330 nm, right *y* axis) and absorption spectra (dashed lines, left *y* axis) are presented. The quantum yield (QY) of the ZnSeS ensemble (with 3-day storage at −30 °C in dark after its synthesis) was estimated to be ~60% (based on this dye in 0.05 M $H_2SO_4$ (lit. QY ~0.546)). TEM images of this ensemble are presented in Figure 4.

The formation of a Se-rich core in the nucleation and early growth stage followed by the formation of an outer layer with an enhanced S amount (as compared to the core) seemed to be a plausible alloying mechanism. Such an alloyed structure, which is inhomogeneous and core−shell-like, was driven by the larger amount of SeDPP used than that of SDPP, together with a greater reactivity of SeDPP than that of SDPP. Subsequently, the amount of ZnSe monomers produced is higher than that of ZnS monomers. Accordingly, it seems reasonable that it is primarily the ZnSe monomer that participates during the nucleation stage (~120 °C), while both the ZnSe and ZnS

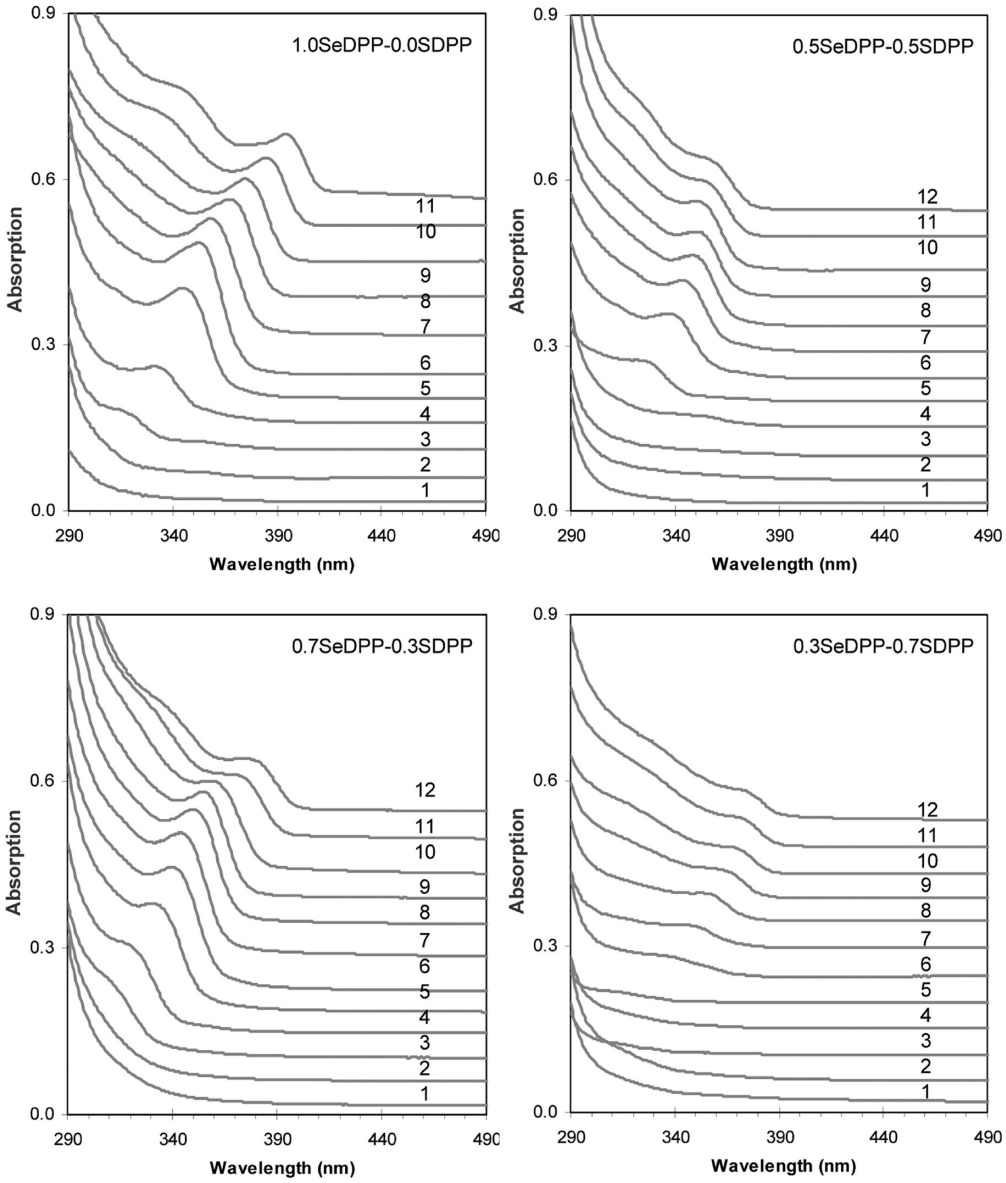


**Figure 2.** Temporal evolution of absorption (offset) of the as-synthesized ZnSe and ZnSeS NCs from four batches in ODE with the precursor feed molar ratios of $4Zn(OA)_2$-1(SeDPP-SDPP). The different SeDPP-SDPP feed molar ratios are indicated. Here, the sample growth periods and temperatures are 45 min/80 °C (sample 1), 15 min/100 °C (sample 2), 15 min/120 °C (sample 3), 15 min/140 °C (sample 4), 15 min/160 °C (sample 5), 15 min/180 °C (sample 6), 15 min/200 °C (sample 7), 15 min/220 °C (sample 8), 15 min/240 °C (sample 9), 15 min/260 °C (sample 10), 15 min/280 °C (sample 11), and 15 min/300 °C (sample 12).

monomers contribute during a later growth stage (~160 °C). The present study on the use of DPP to enhance precursor reactivity to high-quality ZnSeS NCs via a noninjection-based one-pot approach supports a hypothesis, which was proposed based on monomer production rates and which suggests seeded growth and/or nonhot-injection methods to be the strategies to narrow size distribution via extended size focusing.[24,44] Also, the present study brings insight into monomer formation and combination leading to nucleation/growth,[19−25] providing conceptual methodology to various alloyed NCs with high quality, high particle yield, and high synthetic reproducibility.

Figures 2 and 3 demonstrate the temporal evolution of absorption and emission, respectively, of growing ZnSe and ZnSeS NCs from four batches with the feed molar ratios kept as $4Zn(OA)_2$-to-1(SeDPP + SDPP) and [SeDPP+SDPP] of 60 mmol $kg^{-1}$. SeDPP and SDPP stock solutions were mixed and added at 80 °C followed by an addition of 4DPP at the same temperature. Sampling began at 80 °C with subsequent samples taken every 20 °C intervals up to 280 °C (Batch 1.0SeDPP) and 300 °C (the rest three batches). The experimental conditions of the synthetic batches addressed in the present study are also summarized in Table S1 in Supporting Information. Supporting Information Figure S2 shows the comparison of absorption of the same-growth samples from the four batches. Interestingly, nucleation/growth was observed at 100 °C (sample 2) for Batch 1.0SeDPP, 120 °C (Sample 3) for Batch 0.7SeDPP-0.3SDPP, 140 °C (sample 4) for Batch 0.5SeDPP-0.5SDPP, and 160 °C (sample 5) for Batch 0.3SeDPP-0.7SDPP. Thus, the more Se precursor that was present, the earlier nucleation took place. Afterward, the growth of the NCs during the increase of the reaction temperature led to the increase of bandgap emission and the decrease of trap


dx.doi.org/10.1021/am3009828 | ACS Appl. Mater. Interfaces 2012, 4, 4302−4311

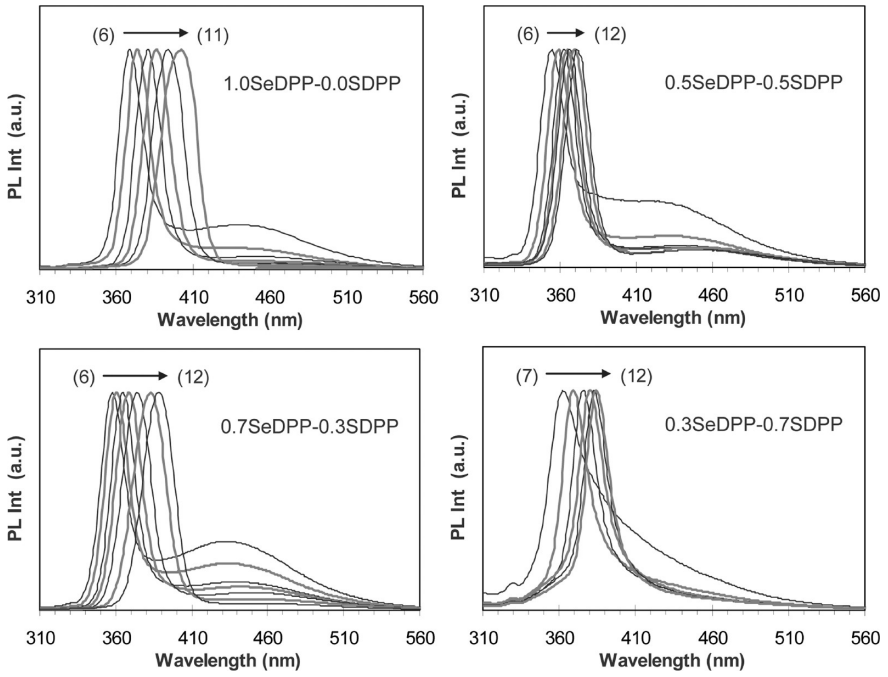


**Figure 3.** Corresponding emission spectra (normalized) of the NC samples labeled from the four batches shown in Figure 2. During the growth, the increase of bandgap emission together with the decrease of trap emission is worthy of notice. See Supporting Information Figure S3 for the comparison of emission peak positions of the last three samples from each of the four batches.

emission, together with the redshift of the bandgap emission peak positions. Such a pattern with an enrichment of bandgap emission accompanied by reduction of trap emission signifies the existence of an annealing process. Note that significant blueshift of bandgap emission during growth was obvious for other NCs, such as ZnCdSe,[29−31] but was not in the present system under the present synthetic condition.

The comparison of the emission peak positions of samples 10−12 (taken at 260−300 °C) from the four batches is shown in Supporting Figure S3, suggesting that the ZnSeS NCs are excellent candidates for the various applications.[2−11] Meanwhile, the blueshift of the bandgap absorption and emission peak positions of the NCs from the batches where SDPP was present, as shown in Figures 2 and 3 and Supporting Informtion Figures S2 and S3, specifies the formation of alloyed ZnSeS NCs.

To further explore the synthesis-structure−property relationships, structural and compositional characterization was performed using TEM, XRD, XPS, and EDX to acquire evidence about the nature of an inhomogeneous but layer-like alloyed structure. Figure 4 shows a dark-field TEM image (top) and a high-resolution TEM image (bottom) of the NCs presented in Figure 1. On the basis of our examination of 278 particles, the diameter of the NCs was estimated to be 3.7 ± 0.3 nm with a size distribution of 8.0%. See Supporting Information Figure S4 for the corresponding size histogram.

Figure 5 displays X-ray diffraction (XRD) patterns of four samples obtained from another batch but with the identical experimental condition as that of Batch 0.7SeDPP-0.3SDPP shown in Figures 2 and 3. But this Figure 5 Batch was five times larger in volume and only four samples were taken with 20 min growth at 160 °C (Sample 1), 200 °C (Sample 2), 260 °C (Sample 3), and 300 °C (Sample 4). The XRD patterns of cubic zincblende bulk ZnS and ZnSe are also presented as references, together with that of ZnSe NCs. For the two types of crystal structures of bulk ZnS of hexagonal wurtzite and cubic zincblende, the latter is the stable structure at room temperature.[45−47] The diffraction peaks are indexed, and the ZnSeS NCs seem to have a zincblende cubic structure.

Also, the diffraction peak positions of the ZnSeS NCs are between those of the binary ZnSe and ZnS materials, indicating that the samples are ternary alloys. Concurrently, from samples 1 to 4, there is an obvious decrease in the fwhm of the diffraction peaks such as (220), suggesting an increase in the NC size. The ZnSeS NC diffraction peaks are fitted readily with Gaussian line shapes because of their symmetry. For samples 1−4, their mean sizes estimated by the Sherrer equation (based on their (220) diffraction peaks with a shape factor of 0.95) are 1.65, 2.04, 2.36, and 2.65 nm, respectively. It is noteworthy that the diffraction peaks of Samples 1 to 4 exhibit very much similar positions, such as (220) at 46.18 ± 0.14. Accordingly, the four ZnSeS samples with the growth between 160 and 300 °C should be similar in composition. Such similarity in composition could be readily understood by the above illustration that, during the nucleation stage (∼120 °C), it is the ZnSe monomer that participates mainly; at a later growth stage (∼160 °C), both the ZnSe and ZnS monomers contribute.

Figure 6 illustrates X-ray photoelectron spectra (XPS) of Sample 4 shown in Figure 5, with a survey scan presented in two parts, 0−270 eV (top-left) and 270−1100 eV (top-right). This survey suggests a possible ternary alloyed nature of Sample 4 with significant amounts of Zn, Se, and S detected. In addition, C and O are abundant, which might be the result of oleic acid as surface ligands. Interestingly, the absence of P implies that DPP should not be the surface ligands for this purified sample, which should be free of any chemicals that are not bonded to nanocrystals. Si was detected and is attributed to our thin sample coverage on a silicon wafer substrate.

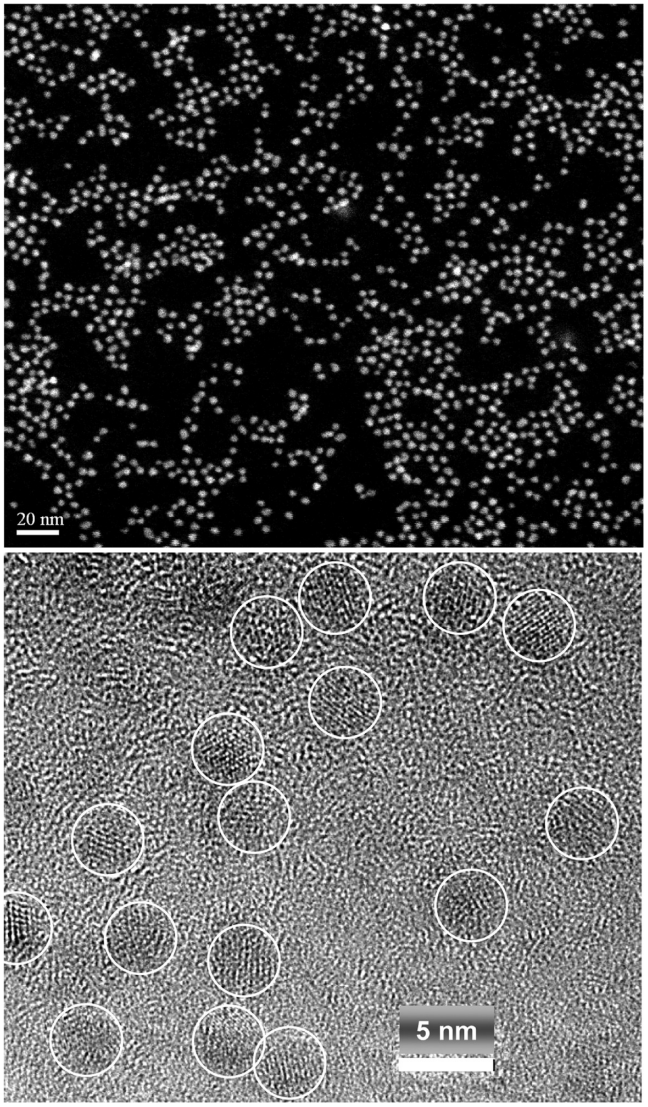


**Figure 4.** Typical TEM images of the ZnSeS QD ensemble shown in Figure 1 after purification. A HAADF-STEM image with a scale bar of 20 nm (top) and a HRTEM image with a scale bar of 5 nm (bottom). The mean size was estimated to be 3.7 ± 0.3 nm.

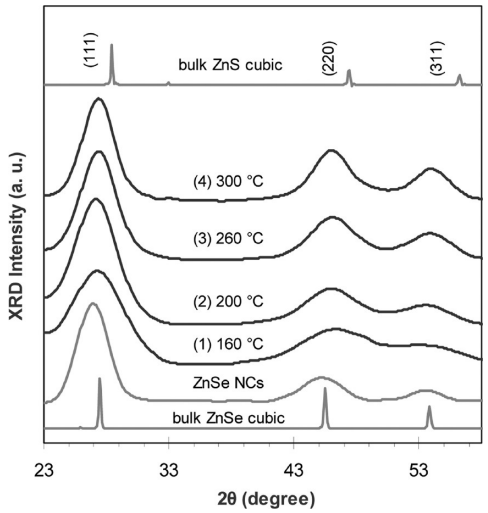


**Figure 5.** Powder XRD patterns of four ZnSeS NC ensembles from one synthetic batch with the precursor feed molar ratio of $4Zn(OA)_2$-0.7SeDPP-0.3SDPP, together with those collected from cubic bulk ZnS and ZnSe and ZnSe NCs. The growth temperatures are designated. The optical properties of the four alloyed samples are presented in Supporting Information Figure S5, demonstrating clearly the redshift and increase of bandgap emission from samples 1−4 accompanied by the decrease of trap emission.

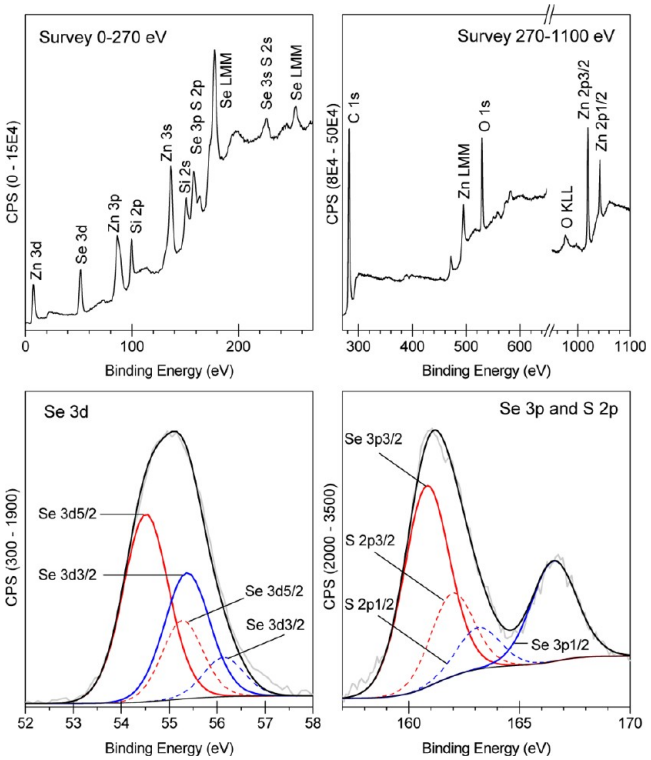


**Figure 6.** An example of XPS study of sample 4 shown in Figure 5. The XPS study illustrates the presence of Zn, Se, and S, together with C and O.

Similar to that reported for CdSe NCs,[48] the Se 3d region (bottom-left) was fitted with two spin−orbit-split doublets by Gaussian−Lorentzian (GL30) line shapes with 1.05 eV fwhm. For the two sets of doublets fitted, they correspond to the contribution from bulk (a lower binding energy Se 3d5/2 peak at 54.4 eV, solid red and blue curves) and surface (a higher binding energy Se 3d5/2 peak at 55.7 eV, dashed red and blue curves). In a same way, the Se 3p and S 2p region (bottom-right) was fitted with two spin−orbit-split doublets, corresponding to Se 3p at 160.8 eV (solid red and blue curves) and S 2p at 162.0 eV (dashed red and blue curves). In these two regions, the gray curves are experimental data, while the black curves symbolize the envelopes of the fitted curves.

The Se 3d region (bottom-left) suggests reasonably the presence of surface Se with a surface-to-bulk ratio of 0.30 for this Sample 4 and 0.47 for Sample 3 (data not shown). In the Se 3p and S 2p region, the Se 3p and S 2p are overlapped, while our fitting seems to designate little or a very tiny surface shift for the two levels. These levels are more deeply bound (with binding energy of 160−168 eV) as compared to the relatively shallow level of Se 3d (with binding energy of ∼55 eV). The observed binding energy for Se 3d, Se 3p, S 2p, and Zn 2p (shown in Supporting Information Figure S6A) are in agreement with literature data.[45,48−52]

Supporting Information Figure S5B-right-top exemplifies the dependence of the S atomic composition x of the four

$ZnSe_{1-x}S_x$ samples addressed in Figure 5 on their lattice constant $a$ (in angstrom Å). The S compositions were determined by both XPS and EDX, and the lattice constants ($a$) were calculated from the (220) diffraction peaks shown in Figure 5. The EDX results are consistent with the XRD results with a small fluctuation in the S composition of 0.25 ± 0.02. The XPS results for samples 3 and 4, $ZnSe_{0.59}S_{0.41}$ and $ZnSe_{0.60}S_{0.40}$, respectively, also indicate little change in the S composition. The discrepancy in the S composition from EDX and XPS supports an inhomogeneous alloyed structure with more S on the outer layer as compared to the center of a NC, due to the fact that XPS is more sensitive to NC surface than EDX. Meanwhile, homogeneous ternary alloys are acknowledged to obey Vegard's law, which displays a linear relationship between alloy composition (expressed as atomic percentage) and lattice parameter.[14,15,17,29,53−55] Accordingly, the ZnSeS QDs presented in Figure 5 are not homogeneous in composition, neither are the other samples shown in Figures 1−3 and Supporting Information Figure S6B.

The optical properties of the four alloyed samples addressed in Figure 5 are presented in Supporting Information Figure S5. From 160 °C-growth sample 1 to 300 °C-growth sample 4 shown in Supporting Information Figure S5, the significant increase of bandgap emission efficiency accompanied by redshift and the decrease of trap emission is worthy of notice. Such a development pattern of the optical properties should be resulted from an annealing process and an increase in NC sizes. These alloyed NCs, samples 1−4, consist of a Se-rich core and a shell with an enhanced S amount.

Note that the EDX S atomic composition (0.25 ± 0.02) of the four ZnSeS samples from the Figure 5 batch seems to be slightly less than the S amount used with the feed molar ratio of 0.7SeDPP-0.3SDPP. Such a difference seems to be suggestive of high reactivity of both SeDPP and SDPP toward $Zn(OA)_2$ but with the former being more reactive. The combination of the Se-to-S feed molar ratio and the reactivity difference led to an inhomogeneous and core−shell-like structure with more S on the shell as compared to that on the inner core. Such a reactivity difference was investigated further by NMR, with 85% $H_3PO_4$ used as an external standard.

Figure 7 gives out $^{31}P$ NMR spectra with $^{1}H$ decoupling collected in the temperature range of 25−80 °C of the precursors of SDPP (top), SeDPP (middle), and a SeDPP-SDPP mixture (bottom). Toluene-$d_8$ was used as the solvent. Previous study suggested that elemental sulfur oxidized SDPP leading to the formation of diphenyldithiophosphinic acid, $Ph_2P(S)SH$ (~54 ppm in $CD_3Cl$ and ~56 ppm in $CH_2Cl_2$);[56−58] in the present study, it was ~-55 ppm in toluene-$d_8$ detected. Meanwhile, the $^{31}P$ NMR spectra of corresponding individual reactions between $Zn(OA)_2$ with SeDPP (top), SDPP (middle), and a SeDPP-SDPP mixture (bottom) are presented in Figure 8. The chemical shift $\delta$ (ppm) of the compounds labeled, together with that of literature reported (ref 22), is **1** 98.5 ppm (98.9 ppm), **2** 76.5 ppm (77.1 ppm), **4** 27.6 ppm (25.7 ppm), **5** 22.3 ppm (22.0 ppm), and **7** −14.3 ppm (−14.5 ppm). Compounds **3**, **3***, and **6** are unknown. The complete absence of SeDPP at 25 °C in the $4Zn(OA)_2$-1SeDPP mixture is apparent, together with the presence of SDPP at 25 °C in the $4Zn(OA)_2$-1SDPP mixture. Accordingly, Figures 7 and 8 demonstrate the relatively high reactivity of SeDPP as compared to that of SDPP toward $Zn(OA)_2$. Such difference in reactivity could be understood by

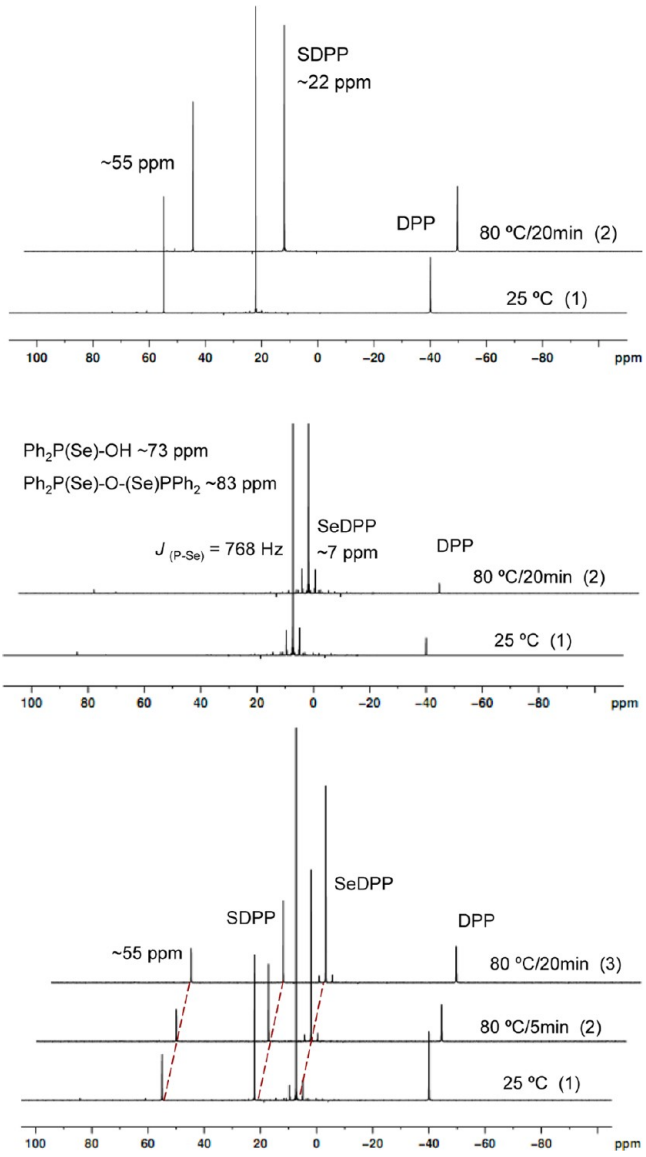


**Figure 7.** $^{31}P$ NMR spectra with $^{1}H$ decoupling of ~0.3 M SDPP (top), ~0.3 M SeDPP (middle), and one 1SeDPP-1SDPP mixture (bottom) collected at the different temperatures indicated. For the two compounds detected at ~73 ppm and ~83 ppm (middle), they were identified according to previous work.[59].

the fact that P═S bond strength is usually stronger than P═Se bond strength.[60]

At the same time, it is worthy of notice that compound **7**, which is $Ph_2P\text{-}PPh_2$,[22,23] was detected to be much more from the $4Zn(OA)_2$-1SeDPP mixture than that from the $4Zn(OA)_2$-1SDPP mixture. Furthermore, compounds **1**, **2**, and **7** were detected in the $4Zn(OA)_2$-1SeDPP mixture (Figure 8 middle) but not in SeDPP (Figure 7 middle). Similarly, Compound 7 was observed in the $4Zn(OA)_2$-1SDPP mixture (Figure 8 top) but not in SDPP (Figure 7 top). Subsequently, it seems that there are no further reactions in the $4Zn(OA)_2$−0.7SeDPP−0.3SDPP mixture (Figure 8 bottom), as compared to those of $4Zn(OA)_2$-1SeDPP (Figure 8 middle) and $4Zn(OA)_2$-1SDPP (Figure 8 top) mixtures. The absence of the additional reactions may be related to the absence of reactions between SeDPP and SDPP; the NMR spectrum of Figure 7 bottom (collected from a 1SeDPP-1SDPP mixture) illustrates a simple

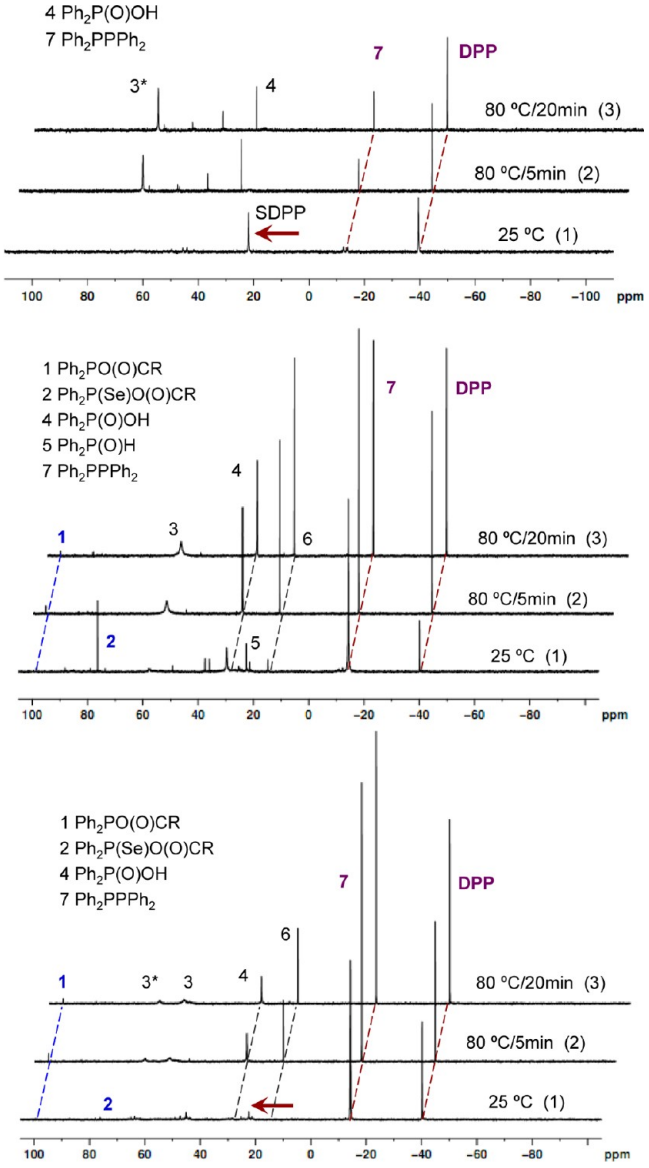


**Figure 8.** $^{31}$P NMR with $^{1}$H decoupling spectra collected from the reactions of 4Zn(OA)$_2$−1SDPP (top), 4Zn(OA)$_2$−1SeDPP (middle), and 4Zn(OA)$_2$−0.7SeDPP-0.3SDPP (bottom).

superimposition of Figure 7 top (SDPP) and Figure 7 middle (SeDPP). Similarly, the NMR spectrum in the bottom part of Figure 8 seems to be a simply overlay of the top (4Zn(OA)$_2$-1SDPP) and middle (4Zn(OA)$_2$-1SeDPP). Consequently, Figures 7 and 8 convey valuable information on the formation mechanism of the ZnSeS alloyed NCs, namely, the combination of individually formed ZnSe and ZnS monomers leading to nucleation/growth shown in Scheme 1 and Supporting Information Figure S1.

Interestingly, Figures 7 and 8 seem to offer evidence on the formation of compound DPP, during the reactions of Zn(OA)$_2$ and SeDPP or SDPP, in addition to those labeled. Such an observation on the increase of DPP amount seems to be consistent with those reported before.[19,22] Different opinions on the formation mechanisms of monomers were expressed, and the present study does not address further such a complicated debate.[19,20,22,23,25,61,62] However, it would be helpful to point out that the formation of DPP together with compound **1** could be resulted from a reaction between Ph$_2$P−PPh$_2$ (compound 7) and one long-chain carboxylic acid RCOOD, as presented in Figure 9A.[63,64] Such an acid, oleic acid, could be resulted from the formation of the monomers. The two values of $J_{(P-D)}$ obtained, 74.5 and 33.3 Hz, from Ph$_2$P(O)D (19.9 ppm, triplet) and Ph$_2$PD (−41.5 ppm, triplet), respectively, are in agreement of literature reported

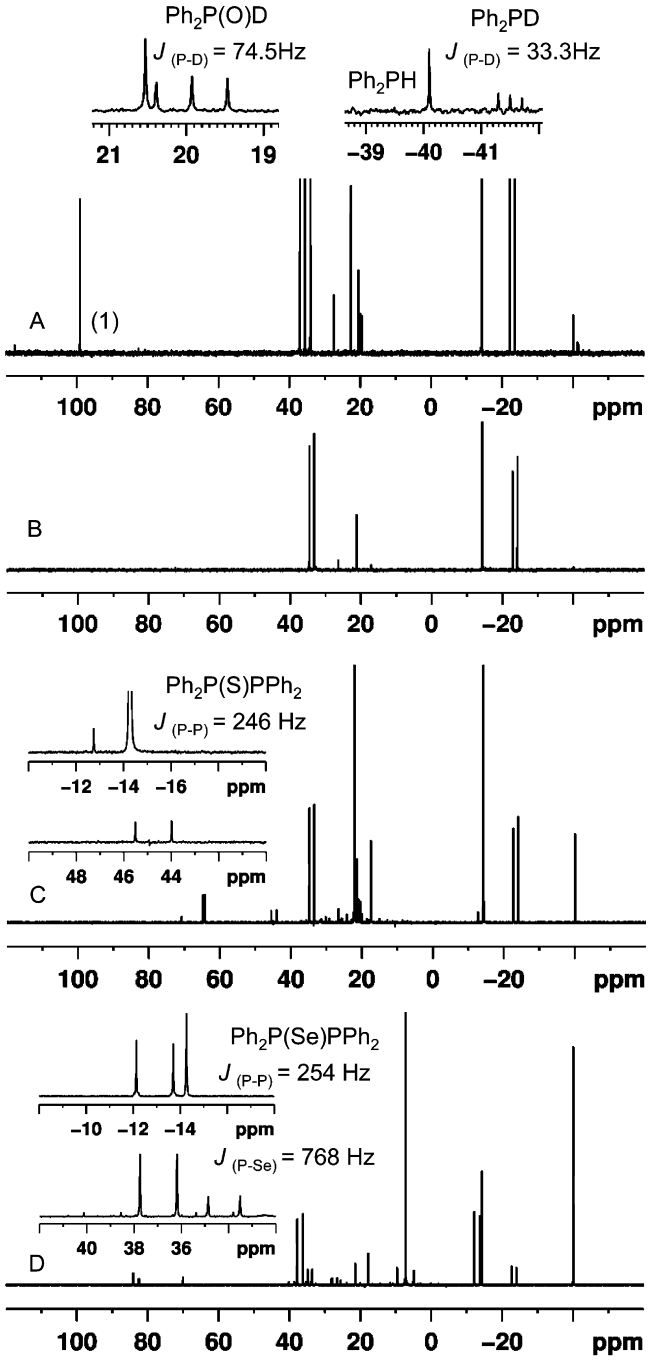


**Figure 9.** Investigation on the formation of DPP. $^{31}$P NMR with $^{1}$H decoupling spectra of (B) commercial Ph$_2$P-PPh$_2$ (Sigma-Aldrich, Lot#47496MJV) in $d_8$-toluene, (A) a mixture of Ph$_2$P-PPh$_2$ and C$_{17}$H$_{33}$-COOD (oleic acid, 90%-d) with a 1-to-2 feed molar ratio in $d_8$-toluene at 80 °C for 15 min, (C) a mixture of Ph$_2$P-PPh$_2$ and SDPP, and (D) a mixture of Ph$_2$P-PPh$_2$ and SeDPP. The NMR suggests the formation of DPP from the three reactions of Ph$_2$P-PPh$_2$ + RCOOD ⇔ Ph$_2$P-OOCR + Ph$_2$PD, Ph$_2$P-PPh$_2$ + SDPP ⇔ Ph$_2$P(S)PPh$_2$ + Ph$_2$PH, and Ph$_2$P-PPh2 + SeDPP ⇔ Ph$_2$P(Se)PPh$_2$ + Ph$_2$PH.

values.[64] Here, $Ph_2P(O)H$ was found to be 22.6 ppm, while $Ph_2PH$ −40.1 ppm. Also, the formation of DPP was found from another two reactions, as shown by Figure 9C and 9D, the $^{31}P$ NMR spectra of which were collected from a mixture of $Ph_2P$-$PPh_2$ and SDPP with a 1-to-1 feed molar ratio in $d_8$-toluene at room temperature for 5 h and from a mixture of $Ph_2P$-$PPh_2$ and SeDPP with a 1-to-2 feed molar ratio in $d_8$-toluene at room temperature for 75 min, respectively. Here, $Ph_2P$-$PPh_2$ was used without purification and its purity was estimated to be ∼60%. See Figure S11 for $^{31}P$ NMR of SDPP and SeDPP used for Figure 9. For Figure 9C, 44.8 ppm and −13.5 ppm (estimated due to the overlap with $Ph_2P$-$PPh_2$) are assigned to $Ph_2P(S)PPh_2$ ($Ph_2P(S)$, 44.8 ppm, doublet; $PPh_2$, −13.5 ppm, doublet) with $J_{(P-P)}$ of 246 Hz. Similarly, for Figure 9D, 37.0 ppm and −12.9 ppm are assigned to $Ph_2P(Se)PPh_2$ ($Ph_2P(Se)$, 37.0 ppm, doublet; $PPh_2$, −12.9 ppm, doublet) with $J_{(P-P)}$ of 254 Hz and $J_{(P-Se)}$ of 768 Hz. We have been examining enthusiastically the formation mechanism of the ZnSe and ZnS monomers, as shown in Scheme 1, involving the formation of DPP.

Because of the formation of DPP during the reactions and the presence of DPP in SeDPP or SDPP (as monitored by NMR shown in Figures 7 and 8), the present study investigates further the effect of the addition of DPP, as presented by Supporting Information Figures S7 and S8. Basically, with and without the addition of 4DPP, before, with, and after the addition of the 0.7SeDPP−0.3SDPP mixture, the nucleation/growth of ZnSeS NCs did not exhibit significant difference. Also, the addition temperatures of 80, 200, 240, and 280 °C of the 0.7SeDPP−0.3SDPP mixture did not seem to play an important role on the optical properties of the 280 °C-growth and 300 °C-growth ZnSeS NCs, as shown by Supporting Information Figure S9. Accordingly, the present noninjection-based approach provides a valuable window of experimental conditions, featuring high-quality ZnSeS alloyed NCs exhibiting bright ultraviolet emission with high synthetic reproducibility and large-scale production capability, as shown in Supporting Information Figure S10 with different feed concentrations of the 0.7SeDPP−0.3SDPP mixture in range of 40−120 mmol $kg^{-1}$.

## 3. CONCLUSION

Highly emissive ultraviolet ZnSeS NCs were synthesized via a noninjection one-pot approach in ODE. A secondary phosphine, diphenylphosphine (DPP), was applied to form Se and S precursors, SeDPP and SDPP, respectively. XRD, XPS, EDX and TEM were performed for structural and compositional characterization. A gradiently alloyed structure with a Se-rich core and an enhanced S amount on the outer layer (than in the center region) and is proposed, together with a cubic crystal structure. Meanwhile, $^{31}P$ NMR communicates the high reactivity of both SeDPP and SDPP even at room temperature, with the former higher than the latter toward $Zn(OA)_2$, as well as the formation of $Ph_2P$−$PPh_2$ and DPP during the reactions. Furthermore, $^{31}P$ NMR supports a model proposed on the combination of ZnSe and ZnS monomers leading to nucleation/growth of ZnSeS alloyed NCs. For the present approach with $4Zn(OA)_2$−0.7SeDPP−0.3SDPP feed molar ratios and 80 °C addition temperature (such as shown in Figures 2 and 3), it is the ZnSe monomer that participates mainly in the nucleation stage at ∼120 °C (due to its high degree of supersatuation). Afterward, the growth of the ZnSeS NCs at ∼160 °C and higher temperatures leads to an increase in size but similarity in compositions, which could be described by a core−shell-like structure with a Se-rich center and an enhanced amount of S on the outer shell. Meanwhile, the increase in bandgap emission with the decrease in trap emission suggests the existence of an annealing effect via the addition of both ZnSe and ZnS monomers. The present study on the formation and characterization of ultraviolet emissive ZnSeS NCs via a noninjection-based one-pot approach featuring high synthetic reproducibility brings insight into the formation mechanism of NC alloys such as ZnSeS via the combination of ZnSe and ZnS monomers. Thus, the present study offers conceptual methodology with high reactivity precursors to various highly photoluminescent alloyed NCs with high quality, high particle yield, and high synthetic reproducibility.

## 4. EXPERIMENTAL SECTION

**4.1. Materials.** All chemicals were commercially available and used without further purification. The chemicals used for reactions include zinc oxide (ZnO, 99.24%) from J.T. Baker Chemical Co. (Philipsburg, NJ, U.S.A.), selenium powder (Se, ∼200 mesh, 99.999%, Alfa Aeser), sulfur (precipitate, Anachemia), diphenylphosphine (DPP, 99%, Strem Chemicals), oleic acid (OA, tech. 90%, Sigma-Aldrich), and 1-octadecene (ODE, tech. 90%, Sigma-Aldrich).

Toluene (99.5%, ACS reagent, ACP in Montreal) was used for optical characterization. Deuterated toluene (toluene-$d_8$, 99.6 atom % D, anhydrous, Sigma-Aldrich) was used for NMR studies. Solvents used for purification were anhydrous, including toluene (99.8%), hexane (≥99%), and methanol (99.8%), which were purchased from Sigma-Aldrich along with acetone (99.5%, ACP in Montreal), which was dried over 4 Å molecular sieves.

**4.2. Synthesis of Nanocrystals.** For a typical synthesis (such as shown in Figures 1−3) with the precursor feed molar ratio of $4Zn(OA)_2$-0.7SeDPP-0.3SDPP and the feed [Se + S] of 60 mmol $kg^{-1}$, 1.839 g (1.205 mmol) $Zn(OA)_2$ stock solution (in ODE with 0.6555 mmol $g^{-1}$), and 3.036 g ODE were loaded in a 50-mL three-necked round-bottom flask equipped with an air-condenser and a thermometer. The mixture was heated to ∼100 °C under vacuum for ∼2 h. The temperature was adjusted to 80 °C (or otherwise specified). A premixed solution, consisting of 0.70 mL (0.20 mmol) SeDPP stock solution (0.29 M in toluene) and 0.12 mL (0.079 mmol) SDPP stock solution (0.66 M in toluene), was then added into the flask. Toluene was removed from the reaction mixture by ∼35 min vacuum. Under a flow of purified $N_2$, the flask was heated up from 80 to 300 °C, with 20 °C increments at a rate of ∼10 °C/min. Twelve samples (∼100 μL each) were taken with their growth periods/temperature of 45 min/80 °C (sample 1), 15 min/100 °C (sample 2), 15 min/120 °C (sample 3), 15 min/140 °C (sample 4), 15 min/160 °C (sample 5), 15 min/180 °C (sample 6), 15 min/200 °C (sample 7), 15 min/220 °C (sample 8), 15 min/240 °C (sample 9), 15 min/260 °C (sample 10), 15 min/280 °C (sample 11), and 15 min/300 °C (sample 12). The optical spectra were collected with a concentration of 10 μL per 3 mL toluene (which means a 10 μL as-synthesized nanocrystal crude solution in 3 mL toluene).

*Preparation of $Zn(OA)_2$ Stock Solution (0.6555 mmol $g^{-1}$).* ZnO (1.1756 g, 14.34 mmol,), oleic acid (8.950 g, 29 mmol), and ODE (12.008 g) were loaded in a three-necked 100-mL round-bottom flask. The mixture was then heated under vacuum to ∼100 °C and degassed for one hour. Then, the mixture was slowly heated to 280−300 °C under a flow of purified nitrogen and stirring. The mixture was kept at this temperature for ∼one hour to ensure a clear solution. Afterward, the solution was cooled to ∼100 °C and degassed for one hour to completely remove any possible moisture. Finally the stock solution was cooled to room temperature under $N_2$ and transferred into a glovebox filled with $N_2$. This stock solution was also used for NMR study.

*Preparation of SeDPP Stock Solution (0.29 M).* In the glovebox, Se powder (0.3556 g, 4.504 mmol) was mixed with DPP (0.80 mL, 4.6 mmol). The mixture in a vial was then heated on a heating mantle

until Se was dissolved and a clear bright yellow liquid was obtained in ~5 min. The vial was then removed from the heating mantle and a white solid (crystal) was formed quickly. The solid was then gently reheated to become liquid, and 15.0 mL anhydrous toluene was added to get a clear solution.

*Preparation of SDPP Stock Solution (0.66 M).* In the glovebox, S powder (0.2424 g, 7.560 mmol) was mixed with DPP (1.31 mL, 7.5 mmol). The mixture in a vial was then heated on a heating mantle until S was dissolved and a clear light yellow liquid was obtained in ~5 min. The vial was then removed from the heating mantle leaving a clear viscous solution. Then, 10.0 mL anhydrous toluene was added to get a clear solution.

*Optical Measurements.* Ultraviolet−visible (UV−vis) absorption spectra were acquired with a Lambda 45 Perkin-Elmer spectrophotometer using a 1-nm data interval. Photoemission spectra were collected with a HORIBA JOBIN YVON FluoroMax-3 spectrofluorometer equipped with a Xenon arc lamp; usually, the increment of 1 nm was applied. The PL QY was estimated by comparing the sample emission intensity with that of quinine sulfate dye in 0.05 M $H_2SO_4$ (lit. QY ~0.546); the optical density at 330 nm of the dye and QD dispersions were controlled to be ~0.1, while the excitation wavelength was 330 nm. The difference of the refractive index of the two solvents was corrected for the estimation.

**4.3. $^{31}$P NMR Experiments.** $^{31}$P NMR was performed on a Bruker AV-III 400 spectrometer operating at 161.98 MHz for $^{31}$P. An external standard 85% $H_3PO_4$ was used when toluene-$d_8$ was not sufficient, namely for spectra examining the reaction between $Zn(OA)_2$ and SeDPP and/or SDPP. Six samples were prepared and the NMR measurements were carried out in the temperature range of 25−80 °C.

*Preparation of SeDPP Stock Solution (0.29 M).* In the glovebox, Se powder (0.0480 g, 0.608 mmol) was mixed with DPP (0.11 mL, 0.63 mmol). The mixture in a vial was then heated on a heating mantle until Se was dissolved and a clear bright yellow liquid was obtained in ~5 min. The vial was then removed from the heating mantle and a white solid (crystal) was formed quickly. The solid was then gently reheated to become liquid, and 2.0 mL toluene-$d_8$ was added to get a clear solution.

*Preparation of SDPP Stock Solution (0.66 M).* In the glovebox, S powder (0.0482 g, 1.50 mmol) was mixed with DPP (0.26 mL, 1.5 mmol). The mixture in a vial was then heated on a heating mantle until S was dissolved and a clear light yellow liquid was obtained in ~5 min. The vial was then removed from the heating mantle leaving a clear viscous solution. Then, 2.0 mL toluene-$d_8$ was added to get a clear solution.

For Figure 7-top SDPP NMR, 0.32 mL SDPP stock solution was added to a 5-mm NMR tube, followed by the addition of 0.48 mL toluene-$d_8$, corresponding to a concentration of 0.26 M. For Figure 7-middle SeDPP NMR, 0.80 mL SeDPP stock solution was added to a 5-mm NMR tube. For Figure 7 -bottom NMR, a mixture of SeDPP and SDPP was prepared by diluting 0.16 mL (0.11 mmol) of SDPP stock solution with 0.24 mL toluene-$d_8$ in a 5-mm NMR tube, followed by the addition of 0.40 mL SeDPP (0.12 mmol) stock solution. Thus, the concentration of [Se + S] was 0.29 M.

For Figure 8-top NMR, 0.8166 g (0.5353 mmol) $Zn(OA)_2$ stock solution (0.6555 mmol/g) in ODE was transferred into a 5-mm NMR tube. 0.18 mL (0.12 mmol) SDPP stock solution was then added to the NMR tube, leading to [S] of ~0.10 M. For Figure 8-middle NMR, 0.5243 g (0.3437 mmol) $Zn(OA)_2$ stock solution (0.6555 mmol/g) in ODE was transferred into a 5-mm NMR tube. 0.27 mL (0.078 mmol) SeDPP stock solution was then added to the NMR tube, leading to [Se] was ~0.10 M. For Figure 8-bottom NMR, 0.2577 g (0.1689 mmol) $Zn(OA)_2$ stock solution (0.6555 mmol $g^{-1}$) in ODE, combined with 0.2543 g ODE, was transferred into a 5-mm NMR tube. 0.10 mL (0.029 mmol) SeDPP stock solution combined with 0.02 mL (0.01 mmol) SDPP stock solution was added to the NMR tube.

**4.4. TEM, EDX XRD, and XPS Characterization.** Intense purification of our NCs was carried out for structural and compositional characterization with transmission electron microscopy (TEM), powder X-ray diffraction (XRD), and X-ray photoelectron spectroscopy (XPS). All solvents used were anhydrous. A reaction mixture was dispersed in toluene and then precipitated with the addition of methanol (to a volume ratio of 1:1), centrifuged, and the supernatant was discarded. Repeated once with 1:1 toluene/methanol and once with 1:3 toluene/methanol, and a white solid was resulted. The solid was dispersed in hexane to form a light yellow clear solution, centrifuged, and the supernatant was collected into another centrifuge tube. Afterward, acetone was added (with a volume ratio of 1:3 hexane/acetone), centrifuged, and the precipitated solid was dispersed in a small amount of hexane. After overnight storage at −30 °C, the solution was filtered to remove any appeared solids through a syringe filter (0.22 $\mu$m pore-size) and then the cartridge was washed with ~3 mL hexane (~1 mL x 3 times). The filtrate was collected and concentrated to ~0.5 mL with a flow of $N_2$.

TEM samples were prepared by depositing diluted NC dispersions in hexane onto 400-mesh thin-carbon-coated Cu grids, followed by drying in air. The samples were examined in a JEOL JEM-2100F field emission source TEM equipped with a scanning unit (STEM) operating at 200 kV. For the present study, high angle annular dark field scanning TEM (HAADF-STEM) images (such as Figure 4-left) were obtained using a Gatan ADF detector, and high resolution TEM (HRTEM) images (such as Figure 4-right) were obtained using a Gatan UltraScan 1000 CCD camera. The atomic composition of the NCs was further studied by the energy dispersive X-ray spectroscopy (EDX) in the STEM mode (STEM-EDX) using an Oxford INCA Energy TEM 200 attached to the JEM-2100F. The NC size and standard deviation were obtained by manually analyzing 278 individual NCs.

Powder XRD patterns were recorded at room temperature on a Bruker Axs D8 X-ray diffractometer using Cu K$\alpha$ radiation in a $\theta$−$\theta$ mode. The generator was operated at 40 kV and 40 mA. Data were collected in a range between 5° and 80° ($2\theta$) with a step size of 0.1° and a counting time of 5 s per step. An XRD sample was prepared by depositing a concentrated NC dispersion in hexane on a low background quartz plate.

XPS was performed using a Kratos Axis Ultra XPS equipped with a monochromated Al K$\alpha$ X-ray source. The instrument pressure in the analysis chamber was $2.0 \times 10^{-9}$ Torr during analysis. Survey scans were conducted using a pass energy of 160 eV, while high resolution scans were carried out at 20 eV using an analysis area of approximately $300 \times 700$ $\mu m^2$. Peak fitting was performed using CasaXPS (ver. 2.2.107) data processing software. Shirley background correction procedures were used as provided by CasaXPS. Curve fitting procedures used for high resolution spectra presented in this report employed a Gaussian−Lorentzian function. High resolution analyses were calibrated to adventitious C 1s signal, at 285 eV. Quantification was performed using sensitivity factors provided by CasaXPS's Scofield element library.

## ■ ASSOCIATED CONTENT

### Ⓢ Supporting Information

Summary of the experimental conditions, schematic drawing of nucleation/growth, XPS of the Zn 2p region, additional data on XRD patterns of ZnSeS NCs with varied feed Se-to-S molar ratios, effect of different DPP amounts added, effect of the order of DPP addition, effect of the addition temperatures of SeDPP and SDPP, and effect of feed concentrations of SeDPP and SDPP with and without additional DPP. This material is available free of charge via the Internet at http://pubs.acs.org.

## ■ AUTHOR INFORMATION

### Corresponding Author

*Phone: 1-(613) 993-9273. Fax: 1-(613) 998-7833. E-mail: kui.yu@nrc.ca.

### Notes

The authors declare no competing financial interest.

## ■ ACKNOWLEDGMENTS

The authors would like to acknowledge Dr. Jack Cornett and Mr. Ian Summerell for financial support from Canadian CRTI 3780-2011-30wa-39, CRTI06-023RD, and CRTI 09-511RD, Émilie Gundlach for experimental help, and Dr. Zygmunt Jakubek for PL lifetime measurements.

## ■ REFERENCES

(1) Yu, K.; Hrdina, A.; Zhang, X.; Ouyang, J.; Leek, D. M.; Wu, X.; Gong, M.; Wilkinson, D.; Li, C. *Chem. Commun.* **2011**, *47*, 8811−8813.
(2) Alivisatos, A. P. *Science* **1996**, *271*, 933−937.
(3) Murray, C. B.; Kagan, C. R.; Bawendi, M. G. *Annu. Rev. Mater. Sci.* **2000**, *30*, 545−610.
(4) Bayer, M. *Nature Phys.* **2011**, *7*, 103−104.
(5) Dabbousi, B. O.; Bawendi, M. G.; Onitsuka, O.; Rubner, M. F. *Appl. Phys. Lett.* **1995**, *66*, 1316−1318.
(6) Hines, M. A.; Guyot-Sionnest, P. *J. Phys. Chem. B* **1998**, *102*, 3655−3657.
(7) Eisler, H. J.; Sundar, V. C.; Bawendi, M. G.; Walsh, M.; Smith, H. I.; Klimov, V. *Appl. Phys. Lett.* **2002**, *80*, 4614−4616.
(8) Tan, Z.; Zhang, F.; Zhu, T.; Xu, J.; Wang, A. Y.; Dixon, J. D.; Li, L.; Zhang, Q.; Mohney, S. E.; Ruzyllo, J. *Nano Lett.* **2007**, *7*, 3803−3807.
(9) Qian, L.; Zheng, Y.; Xue, J.; Holloway, P. *Nat. Photonics* **2011**, *5*, 543−548.
(10) Matsuoka, T. *Adv. Mater.* **1996**, *8*, 469−979.
(11) Gaul, D. A.; Rees, W. S., Jr *Adv. Mater.* **2000**, *12*, 935−946.
(12) Ouyang, J.; Schuurmans, C.; Zhang, Y.; Nagelkerke, R.; Wu, X.; Kingston, D.; Wang, Z. Y.; Wilkinson, D.; Li, C.; Leek, D. M.; Tao, Y.; Yu, K. *ACS Appl. Mater. Interfaces* **2011**, *3*, 553−565.
(13) Yu, K.; Ouyang, J.; Leek, D. M. *Small* **2011**, *7*, 2250−2262.
(14) Yu, K.; Ouyang, J.; Zhang, Y.; Tung, H. T.; Lin, S.; Nagelkerke, R.; Kingston, D.; Wu, X.; Leek, M. D.; Wilkinson, D.; Li, C.; Chen, I. G.; Tao, Y. *ACS Appl. Mater. Interfaces* **2011**, *3*, 1511−1520.
(15) Ouyang, J.; Ratcliffe, C. I.; Kingston, D.; Wilkinson, B.; Kuijper, J.; Wu, X.; Ripmeester, J. A.; Yu, K. *J. Phys. Chem. C* **2008**, *112*, 4908−4909.
(16) Wang, R.; Calvignanello, O.; Ratcliffe, C. I.; Wu, X.; Leek, M. D.; Zaman, Md. B.; Kingston, D.; Ripmeester, J.; Yu, K. *J. Phys. Chem. C* **2009**, *113*, 3402−3408.
(17) Ouyang, J.; Vincent, M.; Descours, P.; Boivineau, T.; Kingston, D.; Zaman, Md. B.; Wu, X.; Yu, K. *J. Phys. Chem. C* **2009**, *113*, 5193−5200.
(18) van Embden, J.; Mulvaney, P. *Langmuir* **2005**, *21*, 10226−10233.
(19) Steckel, J. S.; Yen, B. K. H.; Oertel, D. C.; Bawendi, M. G. *J. Am. Chem. Soc.* **2006**, *128*, 13032−13033.
(20) Liu, H.; Owen, J. S.; Alivisatos, A. P. *J. Am. Chem. Soc.* **2007**, *129*, 305−312.
(21) Rempel, J. Y.; Bawendi, M. G.; Jensen, K. F. *J. Am. Chem. Soc.* **2009**, *131*, 4479−4489.
(22) Evans, C. M.; Evans, M. E.; Krauss, T. D. *J. Am. Chem. Soc.* **2010**, *132*, 10973−10975.
(23) Cossairt, B. M.; Owen, J. S. *Chem. Mater.* **2011**, *23*, 3114−3119.
(24) Clark, M. D.; Kumar, S. K.; Owen, J. S.; Chan, E. M. *Nano Lett.* **2011**, *11*, 1976−1980.
(25) Yu, K. *Adv. Mater.* **2012**, *24*, 1123−1132.
(26) Ma, W.; Luther, J. M.; Zheng, H.; Wu, Y.; Alivisatos, A. P. *Nano Lett.* **2009**, *9*, 1699−1703.
(27) Regulacio, M. D.; Han, M. Y. *Acc. Chem. Res.* **2010**, *43*, 621−630.
(28) Zhong, X. H.; Feng, Y. Y.; Knoll, W.; Han, M. Y. *J. Am. Chem. Soc.* **2003**, *125*, 13559−13563.
(29) Zhong, X. H.; Han, M. Y.; Dong, Z. L.; White, T. J.; Knoll, W. *J. Am. Chem. Soc.* **2003**, *125*, 8589−8594.
(30) Lee, H.; Yang, H.; Holloway, P. H. *J. Lumin.* **2007**, *126*, 314−318.
(31) Protière, M.; Reiss, P. *Small* **2007**, *3*, 399−403.
(32) Wang, X.; Ren, X.; Kahen, K.; Hahn, M. A.; Rajeswaran, M.; Maccagnano-Zacher, S.; Silcox, J; Cragg, G., E.; Efros, A. L.; Krauss, T. D. *Nature* **2009**, *495*, 686−689.
(33) Jang, E.; Jun, S.; Pu, L. *Chem. Commun.* **2003**, 2964−2965.
(34) Swafford, L. A.; Weigand, L. A., II; Bowers, M. J.; McBride, J. R.; Rapaport, J. L.; Watt, T. L.; Dixit, S. K.; Feldman, L. C.; Rosenthal, S. J. *J. Am. Chem. Soc.* **2006**, *128*, 12299−12306.
(35) Bailey, R. E.; Nie, S. M. *J. Am. Chem. Soc.* **2003**, *125*, 7100−7106.
(36) Bae, W. K.; Char, K.; Hur, H.; Lee, S. *Chem. Mater.* **2008**, *20*, 513−539.
(37) Bernard, J. E.; Zunger, A. *Phys. Rev. B* **1986**, *34*, 5992−5995.
(38) Karan, N. S.; Sarma, D. D.; Kadam, R. M.; Pradhan, N. *J. Phys. Chem. Lett.* **2010**, *1*, 2863−2866.
(39) Li, H.; Zanella, M.; Genovese, A.; Povia, M.; Falqui, A.; Giannini, C.; Manna, L. *Nano Lett.* **2011**, *11*, 4964−4970.
(40) Reiss, P. *New J. Chem.* **2007**, *31*, 1843−1852.
(41) Yu, K.; Ouyang, J.; Vincent, M.; Chabloz, D.; Wilkinson, B.; Perier, F. In *Doped Nanomaterials and Nanodevices*; American Scientific Publishers: Stevenson Ranch, CA, USA, 2010; p 175−199.
(42) Yoffe, A. D. *Adv. Phys.* **1993**, *42*, 173−266.
(43) Hernandez-Calderon, I. In *II−VI Semiconductor Materials and Their Applications (Optoelectronic Properties of Semiconductors and Superlattices)*; Taylor & Francis Inc: New York, NY, USA, 2002: p 136−138.
(44) Sugimoto, T. *Adv. Colloid Interface Sci.* **1987**, *28*, 65−108.
(45) Qiao, Z. P.; Xie, G.; Tao, J.; Nie, Z. Y.; Lin, Y. Z.; Chen, X. M. *J. Solid State Chem.* **2002**, *166*, 49−52.
(46) Ma, C.; Moore, D.; Li, J.; Wang, Z. L. *Adv. Mater.* **2003**, *15*, 228−231.
(47) Dawood, F.; Schaak, R. E. *J. Am. Chem. Soc.* **2009**, *131*, 424−425.
(48) Jasieniak, J.; Mulvaney, P. *J. Am. Chem. Soc.* **2007**, *129*, 2841−2848.
(49) Khawaja, E. E.; Durrani, S. M. A.; Hallak, A. B.; Salim, M. A.; Hussain, M. S. *J. Phys. D: Appl. Phys.* **1994**, *27*, 1008−1013.
(50) Winkler, U.; Eich, D; Chen, Z. H.; Fink, R.; Kulkarni, S. K.; Umbach, E. *Chem. Phys. Lett.* **1999**, *306*, 95−102.
(51) Wang, H.; Chen, Z.; Cheng, Q.; Yuan, L. *J. Alloys Compd.* **2009**, *478*, 872−875.
(52) Sarma, D. D.; Nag, A.; Santra, P. K.; Kumar, A.; Sapra, S.; Mahadevan, P. *J. Phys. Chem. Lett.* **2010**, *1*, 2149−2153.
(53) Vegard, L. *Z. Physik* **1921**, *5*, 17−26.
(54) Vegard, L. *Z. Kristallogr.* **1928**, *67*, 239−259.
(55) Furdyna, J. K. *J. Appl. Phys.* **1988**, *64*, R29−64.
(56) Peters, G. *J. Org. Chem.* **1962**, *27*, 2198−2201.
(57) Zukerman-Schpector, J.; Vazquez-Lopez, E. M.; Sanchez, A.; Casas, J. S.; Sordo, J. *J. Organomet. Chem.* **1991**, *405*, 67−74.
(58) Chaudhury, S.; Jain, V. K.; Jakkal, V .S.; Venkatasubramanian, K. *J. Organomet. Chem.* **1992**, *424*, 115−125.
(59) Pilkington, M. J.; Slawin, A. M. Z.; Williams, D. J.; Woollins, J. D. *Main Group Chem.* **1995**, *1*, 145−151.
(60) McDonough, J. E.; Mendiratta, A.; Curley, J. J.; Fortman, G. C.; Fantasia, S.; Cummins, C. C.; Rybak-Akimova, E. V.; Nolan, S. P.; Hoff, C. D. *Inorg. Chem.* **2008**, *47*, 2133−2141.
(61) Garcia-Rodriguez, R.; Liu, H. *J. Am. Chem. Soc.* **2012**, *134*, 1400−1403.
(62) Wang, F.; Buhro, W. R. *J. Am. Chem. Soc.* **2012**, *134*, 5369−5380.
(63) Davidson, R. S.; Sheldon, R. A.; Trippett, S. *J. Chem. Soc. C* **1967**, 1547−1552.
(64) Wong, S. K.; Sytnyk, W.; Wang, J. K. S. *Can. J. Chem.* **1971**, 994−1000.